The Hippo Signaling Pathway Regulates Corneal Endothelial Regeneration

Jingbin Zhuang[†,1], Yuli Guo[†1,2], Houjian Zhang[†,2], Meiqin Zhong[1], Xu Hu[1], Lingyu Zhang[1], Jingwen Yu[1], Yuqian Wang[1], Shundong Cai[1], Huping Wu[1], Chengchao Chu[1], Weifu Huang[4], Andrew J. Quantock[5], Zuguo Liu[*,1,2,3], Wei Li[*,1,3]

[1] Xiamen University Affiliated Xiamen Eye Center, Fujian Provincial Key Laboratory of Ophthalmology and Visual Science; Fujian Engineering and Research Center of Eye Regenerative Medicine; Eye Institute of Xiamen University; School of Medicine, Xiamen University; Xiamen, China.

[2] Department of Ophthalmology, the First Affiliated Hospital of University of South China; Hengyang, Hunan, China.

[3] Department of Ophthalmology, Xiang'an Hospital of Xiamen University, School of Medicine, Xiamen University; Xiamen, China.

[4] TowardPi Medical Technology Beijing; Beijing, China.

[5] School of Optometry and Vision Sciences, Cardiff University, Cardiff, UK.

† These authors contributed equally to this work.

[*] Corresponding author:

Wei Li: Eye Institute of Xiamen University, Fujian Provincial Key Laboratory of Ophthalmology and Visual Science, School of Medicine, Xiamen University, 405, Chengyi Build, Xiang-an campus of Xiamen University, South Xiang-an Road, Xiamen, Fujian, 361102, China. Email: wei1018@xmu.edu.cn

Zuguo Liu: Department of Ophthalmology, Xiang'an Hospital and Xiamen Eye Center affiliated to Xiamen University, Eye Institute of Xiamen University, Fujian Provincial Key Laboratory of Ophthalmology and Visual Science, Fujian Engineering and Research Center of Eye Regenerative Medicine, Xiamen, Fujian, 361102, China. Email: zuguoliu@xmu.edu.cn

Abstract

Corneal endothelial cells (CECs) have limited regeneration capacity in primates while display a potent restorative capability in some species such as rodents after wounding. The mechanism which determines the regenerative capability of CECs remains poorly understood. Here, we identified that the Hippo pathway was inhibited and the downstream effector YAP was activated during CEC wound healing in rabbits. Knockdown of *Yap1* and pharmacological inhibition of YAP suppressed CECs wound healing in rodents in both *in vitro* and *in vivo* models. XMU-MP-1, a specific small molecular inhibitor for Hippo pathway, could promote the corneal endothelial regeneration in rodents and corneal endothelial proliferation in cultured primate CECs, as well as *in vivo* non-human primate CEC wounding model. These findings suggest that Hippo pathway serves as a conserved signal to regulate corneal endothelial regeneration among various species, providing a novel target for non-invasive treatment of corneal endothelium decompensation.

Key words: Corneal endothelium, regeneration, Hippo, YAP

One Sentence Summary: The Hippo pathway regulates corneal endothelial regeneration across species, revealing a therapeutic strategy for corneal endothelial decompensation.

INTRODUCTION

The inner surface of cornea consists a single layer of hexagonal corneal endothelial cells (CECs) which maintain hydration and transparency of cornea through barrier function and pump function of CECs (*1, 2*). The normal density of CEC in adult humans is 2500 cells/mm^2 in average (*3*). When CEC density falls below a critical threshold around 500 cells/mm^2, the corneal endothelial function will be decompensated, with the result of corneal edema, opacity and progressive vision loss (*4, 5*), constituting one of the leading causes of corneal blindness (*6*).

Currently, surgical treatment is the major therapeutic approach for corneal endothelial decompensation, including Descemet stripping endothelial keratoplasty and Descemet's membrane endothelial keratoplasty (*7, 8*). However, it is limited by global shortage of corneal donor tissue. Several researches tried to transplant cultured human CECs (*9, 10*) and human pluripotent stem cell derived CECs (*11*) to replenish the lost CECs. A series of studies on animal models (*12-15*) and clinical trials (*16-18*) have shown that Rho-kinase inhibitors (ROCKi) could promote CEC wound healing. However, there are currently no pharmaceutical interventions clinically approved for corneal endothelial decompensation.

The regenerative capacity of CEC varies among species. Although CECs in primates exhibit limited *in vivo* proliferation capacity, CECs in rodents such as rabbit and mouse demonstrate a robust ability to regenerate (*19, 20*), while underneath mechanism is poorly understood. Over the past few years, tissues from other species possessing regenerative capability have been extensively utilized to study the molecular mechanism, contributing to identification of novel pharmaceutical targets to treat human diseases (*21-23*). Therefore, investigating the mechanism of corneal endothelial wound healing in rodents may provide insights for exploring strategies for human corneal endothelial regeneration.

The Hippo pathway has been reported to play a crucial role in tissue wound healing and organ development and regeneration (*24-27*). It function via a phosphorylation cascade involving MST1/2, LATS1/2, and MOB1A/B proteins, which subsequently

79 phosphorylates the downstream transcriptional cofactors YAP/TAZ for their
80 cytoplasmic retention. When the Hippo pathway is inactivated, unphosphorylated
81 YAP/TAZ translocates into the nucleus and initiates transcription of pro-proliferative
82 and pro-survival genes to promote cell regeneration (*28, 29*). In this study, we
83 investigated the role of Hippo signaling pathway on corneal endothelial wound
84 healing and determined whether this signaling pathway can be a regulator of corneal
85 endothelial regeneration in multiple species.
86
87 **RESULTS**
88 **Hippo pathway is a predominant regenerative signal changed during corneal**
89 **endothelial wound healing process**
90 To probe the mechanism of corneal endothelial wound healing in rabbits, we scraped
91 the central CECs and performed RNA-sequencing on CECs from central area and
92 peripheral area during the process of wound healing on day 7 (Fig.1A). 354 genes
93 were upregulated and 475 genes were downregulated in CECs from central area (D7C)
94 compared with that of peripheral area (D7P) (Fig.1B). Kyoto Encyclopedia of Genes
95 and Genomes (KEGG) enrichment analysis revealed that the differentially expressed
96 genes (DEGs) were predominantly associated with extracellular matrix
97 (ECM)-receptor interaction, focal adhesion, cell cycle, p53 pathway as well as Hippo
98 signaling pathway (Fig.1C). Protein-Protein Interaction Networks (PPI) showed that
99 the core proteins of the top 100 pairs of interactions include CDK1, BUB1, PLK2,
100 NDC80, CDKN1A, CCNB1, AURKB, LRGUK, BMP4 and TOP2A (Fig.1D), and the
101 corresponded genes were mostly cell cycle-related genes. Notably, majority of these
102 genes are downstream genes of Hippo-YAP pathway (*30*). KEGG enrichment for
103 genes related to the top 100 of PPIs also showed significant enrichment in the Hippo
104 signaling pathway (Fig.1E), which has been reported to regulate mitotic cell cycle in
105 mammals (*31-34*). Additionally, uninjured central CECs (D0C) and fully recovered
106 CECs (D14C) were subjected to RNA-sequencing. Downstream genes of the Hippo
107 pathway exhibited significant upregulation during CEC regeneration and
108 downregulation upon completion of wound healing in rabbit (Fig.1F).

We further investigated the function of Hippo pathway in CEC wound healing across species using a rabbit CEC cryoinjury model, a mouse UV-induced CEC damage model, and an *in vitro* primary monkey CEC scraping model. YAP phosphorylation was significantly decreased on day 7 and returned to baseline level on day 14 after CEC cryoinjury in rabbit (Fig.1, G and H). Phosphorylated MST1 and LATS1, two key kinases in the Hippo pathway, showed similar pattern (Fig.1, G and H). There was obvious YAP nuclear translocation on day 7 compared to day 0 (Fig.1I). Similar finding was also detected during wound healing of UV-induced mouse CEC damage (fig.S1, A and B) and the primary monkey CEC scraping model (fig.S1, C to E). Collectively, these results indicated that the Hippo pathway was downregulated and YAP was activated during CEC wound healing in different species.

Hippo pathway is a major regulator of CEC regeneration

To elucidate the role of Hippo pathway in CEC regeneration, we applied verteporfin, a specific inhibitor of YAP which disrupts the YAP-TEAD interaction (*35*), to block YAP function. EdU labeling and Ki67 staining showed reduced proliferation of primary rabbit CECs under verteporfin treatment (Fig.2A). CCK8 assay showed that verteporfin inhibited viability of primary rabbit CECs in a dose-dependent manner (Fig.2B). Human CEC line B4G12 demonstrated similar changes after YAP inhibition (fig.S2). Verteporfin eye drops were subsequently administrated to treat rabbits following corneal endothelial cryoinjury, and the cornea showed reduced transparency on day 7 and cloudy central cornea on day 13 (Fig.2, C and F). Anterior segment optical coherence tomography (OCT) examination showed delayed recovery of corneal edema in verteporfin treated rabbit (Fig.2, D and F). Alizarin red staining of rabbit corneas on day 13 confirmed delayed CEC wound healing after verteporfin application, characterized by absence of cellular structure in the central corneal endothelium (Fig.2E). Similar results were observed in mouse with UV radiation induced corneal endothelial damage (Fig.2, G to J). Putting together, pharmacological YAP inhibition suppressed the regeneration of CECs in both *in vitro* and *in vivo* models across species.

139 To further confirm the function of YAP in corneal endothelium, primary rabbit
140 CECs were transfected with a siRNA specific to *Yap1*. EdU and Ki67 positive cells
141 were significantly reduced after knockdown of *Yap1* (Fig.2, K, L and N). Cell
142 viability was also reduced after knockdown of *Yap1* as measured by CCK8 assay (Fig.
143 2M). Similar results were observed in B4G12 cell line (fig.S3). Next, we determined
144 the effect of *Yap1* knockdown on wound healing in a mouse model. The
145 adeno-associated virus (AAV) vector carrying *Yap1*-specific short hairpin RNA
146 (AAV-*Yap1*-shRNA) was injected into mouse anterior chamber and verified by
147 ZsGreen expression in the corneal endothelium 4 weeks after injection (Fig. 2O).
148 *Yap1* mRNA expression was suppressed in the corneal endothelium of
149 AAV-*Yap1*-shRNA mice (Fig. 2P), and the mice showed a delayed recovery from
150 corneal opaque and stromal edema after UV radiation damage (Fig.2, Q, R and T).
151 Taken together, pharmacological YAP inhibition and *Yap1* knockdown significantly
152 suppressed corneal endothelial regeneration, supporting the function of Hippo
153 signaling pathway in corneal endothelial wound healing.
154
155 **Pharmaceutical inhibition of Hippo pathway with XMU-MP-1 promotes CEC**
156 **regeneration**
157 XMU-MP-1, a specific MST1/2 inhibitor (*36*), can block Hippo pathway and restrain
158 the phosphorylation of YAP. We applied XMU-MP-1 in primary rabbit CEC culture
159 and found it can reduce YAP phosphorylation and enhance YAP nuclear translocation
160 in rabbit CECs (fig.S4, A, C, E and F). Additionally, XMU-MP-1 increased EdU and
161 Ki67 positive cells in both rabbit CECs (Fig.3, A and B) and human B4G12 cell line
162 (fig.S5, A to D), and enhanced the cell viability (Fig.3C and fig.S5E). Cell cycle
163 analysis revealed a significant decrease of cells in G1-phase and increase of cells in
164 G2/M-phase after XMU-MP-1 application (fig.S6, A and B). XMU-MP-1 treatment
165 also upregulated the expression of cell cycle-related genes including E2F1, CCND1,
166 CCND3, CCNA2 and CCNE1 (fig.S6, C and D).
167 Furthermore, XMU-MP-1 was topically applied in corneal endothelial wound
168 models and found it expedited corneal endothelial wound healing and corneal edema
169 recovery in both rabbits (Fig.3, D to G) and mice (Fig.3, H to K). Immunostaining

170 revealed that XMU-MP-1-treated mouse corneas showed more contiguous ZO-1
171 (Fig.3, L and N) and increased Na^+/K^+-ATPase (Fig.3, M and O) expression.
172 Additionally, more EdU-positive cells were found in the corneal endothelium of
173 XMU-MP-1 treated mice (Fig.3P). These results indicated that XMU-MP-1 could
174 promote CEC regeneration and functional restoration.
175 To verify whether XMU-MP-1 can penetrate the cornea, liquid
176 chromatography-tandem mass spectrometry analysis was utilized to assay the
177 concentration of XMU-MP-1 in the rabbit corneal endothelium 1 hour after topical
178 application, and 2974.44 ± 17.43 ng/g of XMU-MP-1 was detected (fig.S7A). The
179 nuclear translocation of YAP in mouse CECs was also observed following
180 administration of XMU-MP-1 (fig.S7B).
181 We further evaluated the ocular manifestation after 4 weeks topical administration
182 of XMU-MP-1 in normal mice. No corneal limbal neovascularization, corneal
183 epithelial defect or corneal thickness changes were observed after XMU-MP-1
184 application (fig.S8, A and B). There was also no evidence of abnormal tissue
185 proliferation in the conjunctiva, Meibomian glands, or lacrimal glands (fig.S8C).
186 Additionally, there was no significant difference in tear production, intraocular
187 pressure, axial length, or refraction (fig.S8, D to G) compared with that of the control
188 group. There was also no abnormal retinal thickening or neovascularization detected
189 after XMU-MP-1 application (fig.S8, H and I).
190
191 **XMU-MP-1 promotes CEC regeneration in primates**
192 To investigate the effect of XMU-MP-1 on primate CECs, we firstly treated the
193 primary cultured human CECs (Fig.4, A and B) and monkey CECs (Fig.4, C and D)
194 with XMU-MP-1. The results showed that EdU-positive and Ki67-positive cells in
195 both types of CECs increased with XMU-MP-1 administration. Nuclei counting
196 confirmed higher cell density in XMU-MP-1 treated groups despite equal seeding
197 densities (Fig.4, A to D). Next, the XMU-MP-1 treatment was applied to an *ex vivo*
198 monkey corneal endothelial scraping model. Trypan blue staining demonstrated that
199 XMU-MP-1 promoted monkey CEC wound healing, with the defect area completely
200 healed by day 4 post scraping (Fig.4, E and F).
201 Last, XMU-MP-1 solution was topically applied in cynomolgus monkey after
202 cryoinjury of the central corneas. The slit lamp microscopy (Fig.4, G and J) and

203 anterior segment OCT examination (Fig.4, H and K) showed that the corneal
204 transparency and thickness restored to normal in XMU-MP-1 treated eyes at week 3,
205 while one control cornea remained obvious opacity and edema. CECs were observed
206 under in vivo confocal microscopy and regular cell morphology was observed 3
207 weeks after topical application of XMU-MP-1 (Fig.4I). CECs density in the central
208 cornea was restored to pre-injury level with XMU-MP-1 treatment, while it was about
209 half of pre-injury level in control eyes (Fig.4L). These findings suggest that
210 XMU-MP-1 effectively promotes CEC regeneration in primates.
211
212 **DISCUSSION**
213 In this study, we investigated the mechanism involved in CEC regeneration in rabbits
214 and identified Hippo signaling pathway as an important regulator in this process.
215 Hippo pathway inhibitor exhibited efficacy in promoting CEC regeneration across
216 mouse, rabbit and monkey corneal endothelial wounding models, indicating the
217 potential of its clinical application in treating corneal endothelial decompensation.
218 For decades, how to regenerate human CECs has remained a huge challenge.
219 Previous studies have demonstrated that nuclear translocation of YAP is associated
220 with proliferation in primary culture of human CECs (*37, 38*), exogenous YAP could
221 induce cell proliferation in contact-inhibited human CECs monolayers (*39*). However,
222 the role of the Hippo pathway in CEC regeneration in vivo remains unknown. Our
223 results derived in multi-species in vivo demonstrated that CECs regeneration is
224 regulated by the Hippo pathway. In mouse corneal endothelial wounding model,
225 EdU-positive cells were presented at the margin of injured region on day 3 post injury
226 and expanded to nearly the entire damaged region on day 8 (fig.S9A). Nevertheless,
227 no EdU-positive cells were observed in the peripheral corneal endothelium (fig.S9A)
228 and the uninjured corneal endothelium (fig.S9B), indicating the wound healing
229 process initiates in the CECs at the wound margin, and the cell regeneration process is
230 associated with the inactivation of Hippo pathway. Thus we speculate that the
231 inability of human CECs to regenerate may due to evolutionary loss of the capacity to
232 block the Hippo pathway following injury, a capacity which is retained in rodents.
233 Notably, YAP activation is also associated with endothelial-to-mesenchymal
234 transition (EndMT) (*6*), a pathological process during CEC wound healing
235 characterized by upregulation of fibroblast biomarkers (*40*). Our previous study has
236 found that rabbit CECs underwent a transient fibrotic EndMT following injury, and

reversed back to an endothelial phenotype upon completion of wound healing (*40*). In this study, YAP activation has been demonstrated to promote cell cycle progression of CECs, and the CECs morphology could be restored to relatively normal state over time, concomitant with functional recovery of the corneal endothelium (fig.S10). Therefore, EndMT may be also involved in the wound healing of CECs that regulated by YAP.

Although XMU-MP-1 has been shown to effectively promote corneal endothelial regeneration, potential side effects arising from YAP activation (*41*) should be carefully considered. Our evaluation demonstrated that XMU-MP-1 exhibited ocular safety in mice following 4 weeks of topical administration (fig.S8). Besides XMU-MP-1, TRULI and DMX-5804 are also pharmaceutical inhibitors for the Hippo pathway, which inhibit LATS1/2 (*42*) and non-canonical Hippo pathway MAPK4Ks (*43*), respectively. In our study, topical administration of TRULI and DMX-5804 also showed effects in promoting CEC proliferation in vitro and in vivo (fig.S11).

In the monkey experiments, we observed lower cell density and obviously irregular cell morphology in central corneal endothelium of the control group. Although one control cornea restored transparency 3 weeks post injury, which may be due to functional compensation of the surviving CECs, the CEC density of that control cornea did not restore to normal level. In comparison, XMU-MP-1 treatment restored both the cell density and morphology of central CECs to near normal levels, demonstrating the efficacy of XMU-MP-1 in promoting primate CECs regeneration. Based on the results obtained from the control group, it is reasonable to suspect that monkey CECs also possess a weak regenerative capacity in vivo, which is not identical to that of human. Given the difference between animal models and clinical conditions, future clinical study is necessary.

In summary, we identified the Hippo signaling pathway as a regulator for CEC regeneration. Pharmaceutical inhibition of the Hippo pathway promotes corneal endothelial proliferation in multiple corneal endothelial wounding models across species, highlighting its potential for corneal endothelial decompensation treatment.

MATERIALS AND METHODS

Study design

We designed a series of studies to determine the mechanism by which Hippo pathway is involved in regeneration of CECs and to validate the hypothesis that targeting Hippo pathway can effectively promote corneal endothelial regeneration. We first performed RNA-sequencing in a rabbit model of corneal endothelial injury to identify key genes and signaling pathway involved in regeneration of CECs during wound healing. Next, we examined the role of Hippo pathway in corneal endothelial regeneration in cellular and rabbit and mouse models. We then investigated downstream mechanism to determine whether corneal endothelial regeneration was induced by cell cycle mediated by Hippo pathway inhibition. Last, we targeted Hippo pathway in primary culture of rabbit, monkey and human CECs and B4G12 cell line, and in corneal endothelial injury models of rabbit, mouse and monkey to verify whether inhibiting Hippo pathway can promote corneal endothelial regeneration. Animals were randomly assigned to their respective treatment groups. Please refer to the Supplementary Materials for more method details.

Preparation of compounds

The solvent for XMU-MP-1 (MCE, HY-100526) and verteporfin (MCE, HY-B0146) consisted of 5% dimethyl sulfoxide (DMSO, MCE, HY-Y0320C), 20% polyethylene glycol 300 (PEG300, MCE, HY-Y0873) and 75% phosphate buffered solution (PBS, Solarbio, P1020).

Animal

All animals, regardless of gender, were housed in Xiamen University Laboratory Animal Center and maintained under a 12-h light/dark cycle, free access to water and food. Animals used in this study were treated in accordance with the ARVO Statement for the Use of Animals in Ophthalmic and Vision Research. The monkey experiments were performed according to the protocol approved by the Laboratory Animal Management and Ethics Committee of Xiamen University (Approval No. XMULAC20240087).

Animal examination

Corneal images were obtained using the slit-lamp microscope (TAKAGI, 700GL) and high-definition camera (Canon, EOS 7D). Anterior segment OCT images of rabbits and monkeys were obtained by swept-source OCT (TowardPi, Yalkaid YG-100K) and Small Animal Retina Imaging System (Optoprobe) was used for mice. A

301 laser-scanning in vivo confocal microscope with a corneal imaging module
302 (Heidelberg, HRT3-RCM) was used to observe the central CECs of monkeys, and the
303 method of cell counting refers to our previous study (*44*).

304 **Cynomolgus monkey corneal endothelial wound model**

305 Central corneal endothelium damage was performed using transcorneal cryogenic
306 method as previously described (*45*). The corneal endothelium of two cynomolgus
307 monkeys was damaged under general anesthesia by transcorneal freezing with a
308 5-mm-diameter probe for 20 seconds. Before freezing, the copper probe was
309 immersed in liquid nitrogen for 3 minutes to stabilize its temperature at approximately
310 -196℃.

311 To evaluate the effect of XMU-MP-1 on CECs wound healing, XMU-MP-1 (50
312 μM) was topically applied to the right eye of each animal 4 times daily for 3 weeks.
313 Solvent was applied to the lateral eye as a control. The experiments on two eyes were
314 conducted separately to avoid affecting the monkeys in their daily activities.

315 **Rabbit corneal endothelial wound model**

316 The corneal endothelium of New Zealand white rabbits was damaged under general
317 anesthesia by transcorneal freezing with a 6-mm-diameter probe for 15 seconds.
318 XMU-MP-1 (50 μM) or verteporfin (50 μM) was topically applied to rabbit eyes 4
319 times daily after corneal endothelial wounding. For the control group, solvent was
320 administrated.

321 **Mouse corneal endothelial wound model**

322 The UV-induced mouse corneal endothelial injury was performed as previously
323 reported with modification (*46*). In brief, a UVB LED light source (Spectronics
324 Corporation, EB-160C) with an emission peak of 312 nm light, 40 nm bandwidth and
325 irradiance of 620 μW/cm^2 was focused to illuminate a 2-mm-diameter spot onto the
326 mouse cornea for 7 min with the total irradiance energy of 260.4 J/cm^2. After
327 irradiation, 2 μl of XMU-MP-1 (1 μM) or verteporfin (50 μM) was topically applied
328 to mouse eyes 4 times daily, and solvent was applied to the control group.

329 **AAV injection in mouse**

330 For corneal endothelium-specific knockdown of *Yap1*, 8-week-old C57BL/6 mice
331 were anesthetized and anterior chamber was injected with AAV Control-ZsGreen or
332 AAV Yap1 shRNA-ZsGreen (1.3×10^{11} genome copies per eye, Hanbio) using a
333 34-gauge needle. ZsGreen expression was detected in vivo using stereo fluorescence

334 microscope (Leica, M165FC) 4 weeks after injection, then the mice were used to
335 generate corneal endothelial wound model.

336 **Evaluation of corneal transparency**

337 The cornea was observed under slit-lamp microscope and the corneal transparency
338 was evaluated with scores ranged from 0 to 4 as previously reported (*47*): 0, a normal
339 cornea; 0.5, a slight haze visible only under a slit-lamp microscope; 1, a mild haze; 2,
340 a moderate haze with a visible iris; 3, a severe haze with an invisible iris; and 4, a
341 severe haze with corneal ulceration.

342 **Ex vivo monkey corneal endothelial scraping model**

343 Two monkey corneas were divided into 12 equal pieces. After culturing for 24 hours
344 with the endothelial surface facing upward, CECs were scraped off within a 2 mm
345 diameter area using a soft rubber rod. Trypan blue staining was used to visualize areas
346 of endothelial defect. The corneal explants were cultured in Dulbecco's Modified
347 Eagle Medium/Nutrient Mixture F-12 (DMEM/F12, Gibco, 11320033) supplemented
348 with 5% fetal bovine serum (FBS, ABW, AB-FBS-0050), 0.5% DMSO, 2 ng/mL
349 mouse EGF (Gibco, PMG8041), 1% Insulin-Transferrin-Selenium-Ethanolamine
350 (ITS-X, Gibco, A4000046401), 0.5 μg/mL hydrocortisone (Yeasen, 54576ES03) and
351 1% penicillin/streptomycin (P/S, Gibco, 15140-122), with culture medium changed
352 every other day.

353 **Isolation and primary culture of monkey CECs**

354 Monkey CECs were isolated through Descemet's stripping and digestion with 1
355 mg/mL collagenase A (Merck, 10103578001) for 6 h at 37℃. After 5 min in TrypLE
356 (Thermo Fisher Scientific, 12605010) at 37°C, CECs were pelleted at 1200 rpm for 5
357 min and plated on fibronectin coating mix (AthenaES, 0407) treated wells. The cells
358 were cultured in Dulbecco's Modified Eagle Medium (DMEM, Gibco, 11965092)
359 with 10% FBS at 37°C in 5% CO_2.

360 **Isolation and primary culture of human CECs and rabbit CECs**

361 Human tissue was handled according to the Declaration of Helsinki. Corneoscleral
362 tissues from human donor eyes were obtained from the Eye Bank of Xiamen Eye
363 Center of Xiamen University immediately after the central corneal button had been
364 used for corneal transplantation. Human CECs and rabbit CECs were isolated using
365 our previous method (*48*), and the cells were cultured in DMEM/F12 supplemented
366 with 5% FBS, 0.5% DMSO, 2 ng/mL mouse EGF, 1% ITS-X, 0.5 μg/mL

367 hydrocortisone and 1% P/S.

368 **Transfection of rabbit CECs and B4G12 with siRNA**

369 YAP expression was knocked down in rabbit CECs and B4G12 cell line by
370 transfection with the YAP siRNA (Sangon Biotech) using RNATransMate (Sangon
371 Biotech, E607402) following the manufacturer's instruction, with negative control
372 (NC) siRNA as control.

373 **In vitro and in vivo EdU labeling**

374 For *in vitro* EdU labeling, EdU (APExBIO, B8337) was supplemented in the culture
375 medium for a final concentration of 20 mg/ml. Cells were collected after 8 hours
376 labeling.

377 For *in vivo* EdU labeling, mice were given an intraperitoneal injection with 50
378 mg/kg of EdU in sterile PBS for 8 consecutive days. After that, the animals were
379 sacrificed and the corneas were collected for cryosection. EdU signal in corneal
380 endothelium was detected using the Click-iT EdU Alexa Fluor 647 imaging kit
381 (Invitrogen, C10640) according to the manufacturer' s instruction.

382 **RNA sequencing**

383 After general anesthesia, rabbit central CECs with a diameter of 6 mm were scraped
384 off. Corneal endothelium from central and peripheral area was separated for RNA
385 extraction on day 0, day 7 and day 14. Corneal endothelia from six rabbits were
386 pooled into one sample. Total RNA was extracted with Total RNA Extraction Reagent
387 (Abclonal, RK30129) according to the manufacturer's protocol. RNA sequencing
388 analysis was performed on Illumina HiSeq^{TM} 4000 system by Beijing CapitalBio
389 Technology, China. Besides, the RNA was sheared and reverse transcribed to get
390 cDNA used for library construction. After that, sequencing was performed on the
391 prepared library. All the generated raw sequencing reads were filtered to get clean
392 reads stored as FASTQ format. RSEM was used to quantify the Genes expression
393 level (FPKM). DESeq2 package was used for comparative analysis of differences.
394 The screening criteria for differentially expressed genes were |log2FC| >= 1 and
395 p-Value <= 0.05. Gene Ontology (GO) and pathway annotation and enrichment
396 analyses were based on the Gene Ontology Database (http://www.geneontology.org/)
397 and KEGG pathway database (http://www.genome.jp/kegg/), respectively.
398 Bioinformatic analysis was performed using Omicsmart, a dynamic real-time
399 interactive online platform for data analysis (http://www.omicsmart.com).

400 **CCK-8 assay**

401 The CCK-8 solution (Vazyme, A311-01) was added to the culture medium, and the
402 absorbance value (450 nm) for each well was determined 2 hours later using a
403 microplate reader (Thermo, Multiskan GO).

404 **Western blot analysis**

405 Western blot analysis was performed as previously described (*49*). The equal amount
406 of protein was resolved by SDS-PAGE and immunoblotted with primary antibodies
407 for YAP1 (Abclonal, A19134), phospho-YAP1-S127 (Abcam, ab186735), LATS1/2
408 (Proteintech, 17049-1-AP), phospho-LATS1/2 (Thr1079) (Proteintech, 28998-1-AP),
409 MST1/2 (Proteintech, 22245-1-AP), phospho-MST1 (Thr183)/MST2 (Thr180)
410 (Proteintech, 80093-1-RR), MOB1 (Proteintech, 11669-1-AP), phospho-MOB1
411 (Thr12) (Proteintech, 29027-1-AP) and β-actin (Abcam, 8226). Primary antibodies
412 were then detected with HRP-conjugated goat anti-rabbit antibody (Abclonal, AS014),
413 and the band intensity was semiquantified by densitometry using ImageJ software and
414 normalized by β-actin levels.

415 **Quantitative real-time polymerase chain reaction (qRT-PCR)**

416 Total RNA was extracted using Total RNA Extraction Reagent (Abclonal, RK30129),
417 and cDNA was made by using the RT Master Mix for qPCR (Abclonal, RK20433).
418 Real-time qPCR was performed with the SYBR Green qPCR Mix with UDG
419 (Abclonal, RK21219), and the primer sequences are listed in Table S1. The mixture
420 was held at 37°C for 2 min and then heated to 95°C for 3 min, cycled 40 times (95°C
421 for 5 s, 60°C for 30 s). Melting curves were generated by increasing the temperature
422 from 55°C to 95°C in 0.5°C increments at 10 s intervals and then visually to ensure
423 that a single peak was present for each primer. Threshold amplification values (Ct)
424 were assigned by the LightCycler 96 analysis software (Roche).

425 **Immunofluorescence staining on cells and corneal whole mount**

426 Cells or corneas were fixed with 4% paraformaldehyde for 20 min and incubated with
427 2% bovine serum albumin for 60 min to reduce background noise. The cells or
428 corneas were then labeled with primary rabbit antibodies for YAP1 (Abclonal,
429 A19134), Ki67 (Abcam, ab16667), ZO-1 (Invitrogen, 61-7300) or Na^+-K^+ATPase
430 (Abcam, ab76020) overnight at 4°C. After 3 washes with PBS, the samples were
431 incubated with goat anti-rabbit lgG (Abclonal, AS053) for 120 min. The nuclei were
432 stained with DAPI (Beyotime, C1005) for 10 min. The samples were observed under
433 a laser scanning confocal microscopy (ZEISS, LSM880).

434 **Alizarin Red staining**

Mouse or rabbit corneas were incubated with Alizarin Red S solution (Solarbio, G1452) for 5 min. After that, the corneas were fixed with 4% paraformaldehyde for 20 min and cut into flat mount. Images were captured with a microscope (Zeiss, Axio Lab.A1).

Statistical analysis

Statistical analysis was performed using GraphPad Prism software 9.0. Data were presented as mean ± SEM and analyzed by unpaired Student's *t* test for two groups and ANOVA for more than two groups. $P < 0.05$ was considered statistical significant.

References and Notes

1. K. M. Meek, C. Knupp, Corneal structure and transparency. *Prog Retin Eye Res* **49**, 1–16 (2015).
2. G. Suanno, V. G. Genna, E. Maurizi, A. Abu Dieh, M. Griffith, G. Ferrari, Cell therapy in the cornea: The emerging role of microenvironment. *Prog Retin Eye Res* **102**, (2024).
3. W. M. Bourne, Biology of the corneal endothelium in health and disease. *Eye* **17**, 912–918 (2003).
4. K. Gupta, S. X. Deng, Corneal Endothelial Decompensation. *Klin Monatsbl Augenh* **237**, 745–753 (2020).
5. Z. G. He, N. Campolmi, P. Gain, M. H. Binh, J. M. Dumollard, S. Duband, M. Peoc'h, S. Piselli, O. Garraud, G. Thuret, Revisited Microanatomy of the Corneal Endothelial Periphery: New Evidence for Continuous Centripetal Migration of Endothelial Cells in Humans. *Stem Cells* **30**, 2523–2534 (2012).
6. X. Zhang, H. Liu, C. Wan, Y. Li, C. Ren, J. Lu, Y. Liu, Y. Yang, Verteporfin combined with ROCK inhibitor promotes the restoration of corneal endothelial cell dysfunction in rats. *Biochem Pharmacol* **231**, 116641 (2025).
7. A. Viberg, B. Samolov, B. Bystroem, Descemet Stripping Automated Endothelial Keratoplasty versus Descemet Membrane Endothelial Keratoplasty for Fuchs Endothelial Corneal Dystrophy. *Ophthalmology* **130**, 1248–1257 (2023).
8. M. O. Price, P. Calhoun, C. Kollman, F. W. Price, J. H. Lass, Descemet Stripping Endothelial Keratoplasty. *Ophthalmology* **123**, 1421–1427 (2016).
9. S. Kinoshita, N. Koizumi, M. Ueno, N. Okumura, K. Imai, H. Tanaka, Y. Yamamoto, T. Nakamura, T. Inatomi, J. Bush, M. Toda, M. Hagiya, I. Yokota, S. Teramukai, C. Sotozono, J. Hamuro, Injection of Cultured Cells with a ROCK Inhibitor for Bullous Keratopathy. *New Engl J Med* **378**, 995–1003 (2018).
10. K. Numa, K. Imai, M. Ueno, K. Kitazawa, H. Tanaka, J. D. Bush, S. Teramukai, N. Okumura, N. Koizumi, J. Hamuro, C. Sotozono, S. Kinoshita, Five-Year Follow-up of First 11 Patients Undergoing Injection of Cultured Corneal Endothelial Cells for Corneal Endothelial Failure. *Ophthalmology* **128**, 504–514 (2021).
11. Z. Y. Li, H. Y. Duan, Y. N. Jia, C. Zhao, W. J. Li, X. Wang, Y. J. Gong, C. X. Dong, B. C. Ma, S. Q. Dou, B. Zhang, D. F. Li, Y. H. Cao, L. X. Xie, Q. J. Zhou, W. Y. Shi,

Long-term corneal recovery by simultaneous delivery of hPSC-derived corneal endothelial precursors and nicotinamide. *J Clin Invest* **132**, (2022).

12. N. Okumura, S. Nakano, E. P. Kay, R. Numata, A. Ota, Y. Sowa, T. Sakai, M. Ueno, S. Kinoshita, N. Koizumi, Involvement of Cyclin D and p27 in Cell Proliferation Mediated by ROCK Inhibitors Y-27632 and Y-39983 During Corneal Endothelium Wound Healing. *Invest Ophth Vis Sci* **55**, 318–329 (2014).
13. L. C. Meekins, N. Rosado-Adames, R. Maddala, J. J. Zhao, P. V. Rao, N. A. Afshari, Corneal Endothelial Cell Migration and Proliferation Enhanced by Rho Kinase (ROCK) Inhibitors in In Vitro and In Vivo Models. *Invest Ophth Vis Sci* **57**, 6731–6738 (2016).
14. N. Okumura, Y. Okazaki, R. Inoue, K. Kakutani, S. Nakano, S. Kinoshita, N. Koizumi, Effect of the Rho-Associated Kinase Inhibitor Eye Drop (Ripasudil) on Corneal Endothelial Wound Healing. *Invest Ophth Vis Sci* **57**, 1284–1292 (2016).
15. H. Miyagi, S. Kim, J. Li, C. J. Murphy, S. M. Thomasy, Topical Rho-Associated Kinase Inhibitor, Y27632, Accelerates Corneal Endothelial Regeneration in a Canine Cryoinjury Model. *Cornea* **38**, 352–359 (2019).
16. N. Koizumi, N. Okumura, M. Ueno, H. Nakagawa, J. Hamuro, S. Kinoshita, Rho-Associated Kinase Inhibitor Eye Drop Treatment as a Possible Medical Treatment for Fuchs Corneal Dystrophy. *Cornea* **32**, 1167–1170 (2013).
17. G. Moloney, C. Petsoglou, M. Ball, Y. Kerdraon, R. Höllhumer, N. Spiteri, S. Beheregaray, J. Hampson, M. D'Souza, R. N. Devasahayam, Descemetorhexis Without Grafting for Fuchs Endothelial Dystrophy-Supplementation With Topical Ripasudil. *Cornea* **36**, 642–648 (2017).
18. N. Okumura, S. Kinoshita, N. Koizumi, Application of Rho Kinase Inhibitors for the Treatment of Corneal Endothelial Diseases. *J Ophthalmol* **2017**, (2017).
19. W. D. Pei, J. Chen, W. Y. Wu, W. Wei, Y. Yu, Y. Feng, Comparison of the rabbit and human corneal endothelial proteomes regarding proliferative capacity. *Exp Eye Res* **209**, (2021).
20. K. Yoshida, S. Kase, K. Nakayama, H. Nagahama, T. Harada, H. Ikeda, C. Harada, J. Imaki, K. Ohgami, K. Shiratori, I. B. Ilieva, S. Ohno, S. Nishi, K. I. Nakayama, Involvement of p27 in the proliferation of the developing corneal endothelium. *Invest Ophth Vis Sci* **45**, 2163–2167 (2004).
21. S. P. Hui, D. Z. Sheng, K. Sugimoto, A. Gonzalez-Rajal, S. Nakagawa, D. Hesselson, K. Kikuchi, Zebrafish Regulatory T Cells Mediate Organ-Specific Regenerative Programs. *Dev Cell* **43**, 659–+ (2017).
22. P. Lyu, M. Iribarne, D. Serjanov, Y. J. Zhai, T. Hoang, L. J. Campbell, P. Boyd, I. Palazzo, M. Nagashima, N. J. Silva, P. F. Hitchcock, J. Qian, D. R. Hyde, S. Blackshaw, Common and divergent gene regulatory networks control injury-induced and developmental neurogenesis in zebrafish retina. *Nat Commun* **14**, (2023).
23. L. Celotto, F. Rost, A. Machate, J. Bläsche, A. Dahl, A. Weber, S. Hans, M. Brand, Single-cell RNA sequencing unravels the transcriptional network underlying zebrafish retina regeneration. *Elife* **12**, (2023).

24. A. Elbediwy, Z. I. Vincent-Mistiaen, B. Spencer-Dene, R. K. Stone, S. Boeing, S. K. Wculek, J. Cordero, E. H. Tan, R. Ridgway, V. G. Brunton, E. Sahai, H. Gerhardt, A. Behrens, I. Malanchi, O. J. Sansom, B. J. Thompson, Integrin signalling regulates YAP and TAZ to control skin homeostasis. *Development* **143**, 1674–1687 (2016).
25. Z. Liu, H. Wu, K. Jiang, Y. Wang, W. Zhang, Q. Chu, J. Li, H. Huang, T. Cai, H. Ji, C. Yang, N. Tang, MAPK-Mediated YAP Activation Controls Mechanical-Tension-Induced Pulmonary Alveolar Regeneration. *Cell Rep* **16**, 1810–1819 (2016).
26. M. Xin, Y. Kim, L. B. Sutherland, M. Murakami, X. X. Qi, J. McAnally, E. R. Porrello, A. I. Mahmoud, W. Tan, J. M. Shelton, J. A. Richardson, H. A. Sadek, R. Bassel-Duby, E. N. Olson, Hippo pathway effector Yap promotes cardiac regeneration. *P Natl Acad Sci USA* **110**, 13839–13844 (2013).
27. L. Lu, Y. Li, S. M. Kim, W. Bossuyt, P. Liu, Q. Qiu, Y. Wang, G. Halder, M. J. Finegold, J. S. Lee, R. L. Johnson, Hippo signaling is a potent in vivo growth and tumor suppressor pathway in the mammalian liver. *Proc Natl Acad Sci U S A* **107**, 1437–1442 (2010).
28. F. X. Yu, K. L. Guan, The Hippo pathway: regulators and regulations. *Gene Dev* **27**, 355–371 (2013).
29. J. B. Huang, S. Wu, J. Barrera, K. Matthews, D. J. Pan, The Hippo signaling pathway coordinately regulates cell proliferation and apoptosis by inactivating Yorkie, the homolog of YAP. *Cell* **122**, 421–434 (2005).
30. A. Totaro, T. Panciera, S. Piccolo, YAP/TAZ upstream signals and downstream responses. *Nat Cell Biol* **20**, 888–899 (2018).
31. N. R. Kastan, S. Oak, R. Liang, L. Baxt, R. W. Myers, J. Ginn, N. Liverton, D. J. Huggins, J. Pichardo, M. Paul, T. S. Carroll, A. Nagiel, K. Gnedeva, A. J. Hudspeth, Development of an improved inhibitor of Lats kinases to promote regeneration of mammalian organs. *P Natl Acad Sci USA* **119**, (2022).
32. E. Jahanshir, J. Llamas, Y. Kim, K. Biju, S. Oak, K. Gnedeva, The Hippo pathway and p27(Kip1) cooperate to suppress mitotic regeneration in the organ of Corti and the retina. *Proc Natl Acad Sci U S A* **122**, e2411313122 (2025).
33. Y. Morikawa, J. H. Kim, R. G. Li, L. Liu, S. J. Liu, V. Deshmukh, M. C. Hill, J. F. Martin, YAP Overcomes Mechanical Barriers to Induce Mitotic Rounding and Adult Cardiomyocyte Division. *Circulation* **151**, 76–93 (2025).
34. G. Pattschull, S. Walz, M. Gründl, M. Schwab, E. Rühl, A. Baluapuri, A. Cindric-Vranesic, S. Kneitz, E. Wolf, C. P. Ade, A. Rosenwald, B. von Eyss, S. Gaubatz, The Myb-MuvB Complex Is Required for YAP-Dependent Transcription of Mitotic Genes. *Cell Rep* **27**, 3533–+ (2019).
35. A. Perra, M. A. Kowalik, E. Ghiso, G. M. Ledda-Columbano, L. Di Tommaso, M. M. Angioni, C. Raschioni, E. Testore, M. Roncalli, S. Giordano, A. Columbano, YAP activation is an early event and a potential therapeutic target in liver cancer development. *J Hepatol* **61**, 1088–1096 (2014).
36. F. Q. Fan, Z. X. He, L. L. Kong, Q. H. Chen, Q. Yuan, S. H. Zhang, J. J. Ye, H. Liu, X. F. Sun, J. Geng, L. Z. Yuan, L. X. Hong, C. Xiao, W. J. Zhang, X. H. Sun, Y. Z. Li, P. Wang, L. H. Huang, X. R. Wu, Z. L. Ji, Q. Wu, N. S. Xia, N. S. Gray, L. F. Chen, C. H.

563 Yun, X. M. Deng, D. W. Zhou, Pharmacological targeting of kinases MST1 and
564 MST2 augments tissue repair and regeneration. *Sci Transl Med* **8**, (2016).
565 37. Y. T. Zhu, H. C. Chen, S. Y. Chen, S. C. G. Tseng, Nuclear p120 catenin unlocks
566 mitotic block of contact-inhibited human corneal endothelial monolayers
567 without disrupting adherent junctions. *J Cell Sci* **125**, 3636–3648 (2012).
568 38. C. Zhao, Q. J. Zhou, H. Y. Duan, X. Wang, Y. N. Jia, Y. J. Gong, W. J. Li, C. X. Dong,
569 Z. Y. Li, W. Y. Shi, Laminin 511 Precoating Promotes the Functional Recovery of
570 Transplanted Corneal Endothelial Cells. *Tissue Eng Pt A* **26**, 1158–1168 (2020).
571 39. Y. J. Hsueh, H. C. Chen, S. E. Wu, T. K. Wang, J. K. Chen, D. H. K. Ma,
572 Lysophosphatidic acid induces YAP-promoted proliferation of human corneal
573 endothelial cells via PI3K and ROCK pathways. *Mol Ther-Meth Clin D* **2**, (2015).
574 40. J. Chen, Z. Li, L. Zhang, S. Ou, Y. Wang, X. He, D. Zou, C. Jia, Q. Hu, S. Yang, X. Li, J.
575 Li, J. Wang, H. Sun, Y. Chen, Y. T. Zhu, S. C. G. Tseng, Z. Liu, W. Li, Descemet's
576 Membrane Supports Corneal Endothelial Cell Regeneration in Rabbits. *Sci Rep* **7**,
577 6983 (2017).
578 41. I. M. Moya, G. Halder, Hippo-YAP/TAZ signalling in organ regeneration and
579 regenerative medicine. *Nat Rev Mol Cell Bio* **20**, 211–226 (2019).
580 42. N. Kastan, K. Gnedeva, T. Alisch, A. A. Petelski, D. J. Huggins, J. Chiaravalli, A.
581 Aharanov, A. Shakked, E. Tzahor, A. Nagiel, N. Segil, A. J. Hudspeth,
582 Small-molecule inhibition of Lats kinases may promote Yap-dependent
583 proliferation in postmitotic mammalian tissues. *Nat Commun* **12**, (2021).
584 43. L. R. Fiedler, K. Chapman, M. Xie, E. Maifoshie, M. Jenkins, P. A. Golforoush, M.
585 Bellahcene, M. Noseda, D. Faust, A. Jarvis, G. Newton, M. A. Paiva, M. Harada, D. J.
586 Stuckey, W. H. Song, J. Habib, P. Narasimham, R. Aqil, D. Sanmugalingam, R. Yan,
587 L. Pavanello, M. Sano, S. C. Wang, R. D. Sampson, S. Kanayaganam, G. E. Taffet, L.
588 H. Michae, M. L. Entman, T. H. Tan, S. E. Harding, C. M. R. Low, C. Tralau-Stewart,
589 T. Perrior, M. D. Schneider, MAP4K4 Inhibition Promotes Survival of Human Stem
590 Cell-Derived Cardiomyocytes and Reduces Infarct Size. *Cell Stem Cell* **24**, 579–+
591 (2019).
592 44. J. H. Bu, J. W. Yu, Y. Wu, X. X. Cai, K. C. Li, L. Y. Tang, N. Jiang, M. V. Jeyalatha, M. J.
593 Zhang, H. M. Sun, H. He, A. J. Quantock, Y. X. Chen, Z. G. Liu, W. Li,
594 Hyperlipidemia Affects Tight Junctions and Pump Function in the Corneal
595 Endothelium. *Am J Pathol* **190**, 563–576 (2020).
596 45. N. Okumura, N. Koizumi, E. P. Kay, M. Ueno, Y. Sakamoto, S. Nakamura, J.
597 Hamuro, S. Kinoshita, The ROCK Inhibitor Eye Drop Accelerates Corneal
598 Endothelium Wound Healing. *Invest Ophth Vis Sci* **54**, 2493–2502 (2013).
599 46. C. L. Liu, T. Miyajima, G. Melangath, T. Miyai, S. Vasanth, N. Deshpande, V. Kumar,
600 S. O. Tone, R. Gupta, S. Zhu, D. Vojnovic, Y. M. Chen, E. G. Rogan, B. Mondal, M.
601 Zahid, U. V. Jurkunas, Ultraviolet A light induces DNA damage and
602 estrogen-DNA adducts in Fuchs endothelial corneal dystrophy causing females
603 to be more affected. *P Natl Acad Sci USA* **117**, 573–583 (2020).
604 47. C. Zhao, W. Li, H. Duan, Z. Li, Y. Jia, S. Zhang, X. Wang, Q. Zhou, W. Shi, NAD(+)
605 precursors protect corneal endothelial cells from UVB-induced apoptosis. *Am J*
606 *Physiol Cell Physiol* **318**, C796–c805 (2020).

48. W. Li, A. L. Sabater, Y. T. Chen, Y. Hayashida, S. Y. Chen, H. He, S. C. G. Tseng, A novel method of isolation, preservation, and expansion of human corneal endothelial cells. *Invest Ophth Vis Sci* **48**, 614–620 (2007).
49. S. Li, L. Tang, J. Zhou, S. Anchouche, D. Li, Y. Yang, Z. Liu, J. Wu, J. Hu, Y. Zhou, J. Yin, Z. Liu, W. Li, Sleep deprivation induces corneal epithelial progenitor cell over-expansion through disruption of redox homeostasis in the tear film. *Stem Cell Reports* **17**, 1105–1119 (2022).

Acknowledgement: We thank Jingru Huang and Xiang You from Central Lab, School of Medicine, Xiamen University for technical support in confocal imaging. We thank Haiping Zheng from Central Lab, School of Medicine, Xiamen University for technical support in cell cycle analysis.

Funding:

National Natural Science Foundation of China 82471047 (LW)
National Natural Science Foundation of China 81970773 (LW)
National Natural Science Foundation of China 82401223 (GYL)
China Post-doctoral science foundation 2024M751351 (GYL)
China Post-doctoral science foundation 2023M741610 (ZHJ)
China Post-doctoral science foundation BX20240154 (ZHJ)
Natural Science Foundation of Hunan Province, China 2025JJ90130 (GYL)
Natural Science Foundation of Hunan Province, China 2024JJ6403 (ZHJ)

Author contributions: J.Z., Y.G., H.Z. and W.L. designed the overall project and wrote the manuscript, J.Z., Y.G., H.Z., W.H., Y.W., M.Z., X.H., L.Z., J.Y. and S.C. performed the experiments and data analysis. H.W. collected human corneoscleral tissues. Z.L., A.Q, C.C, and W.L. revised the manuscript. J.Z., Y.G., and H.Z. contributed equally to this work, thus should be considered as co-first authors. All authors have reviewed and approved the manuscript.

Competing interests: The authors declare that they have no competing interests.

Data and materials availability: All data associated with this study are present in the paper or the Supplementary Materials. This study did not generate any unique code. Source data are provided with this paper.

Figures

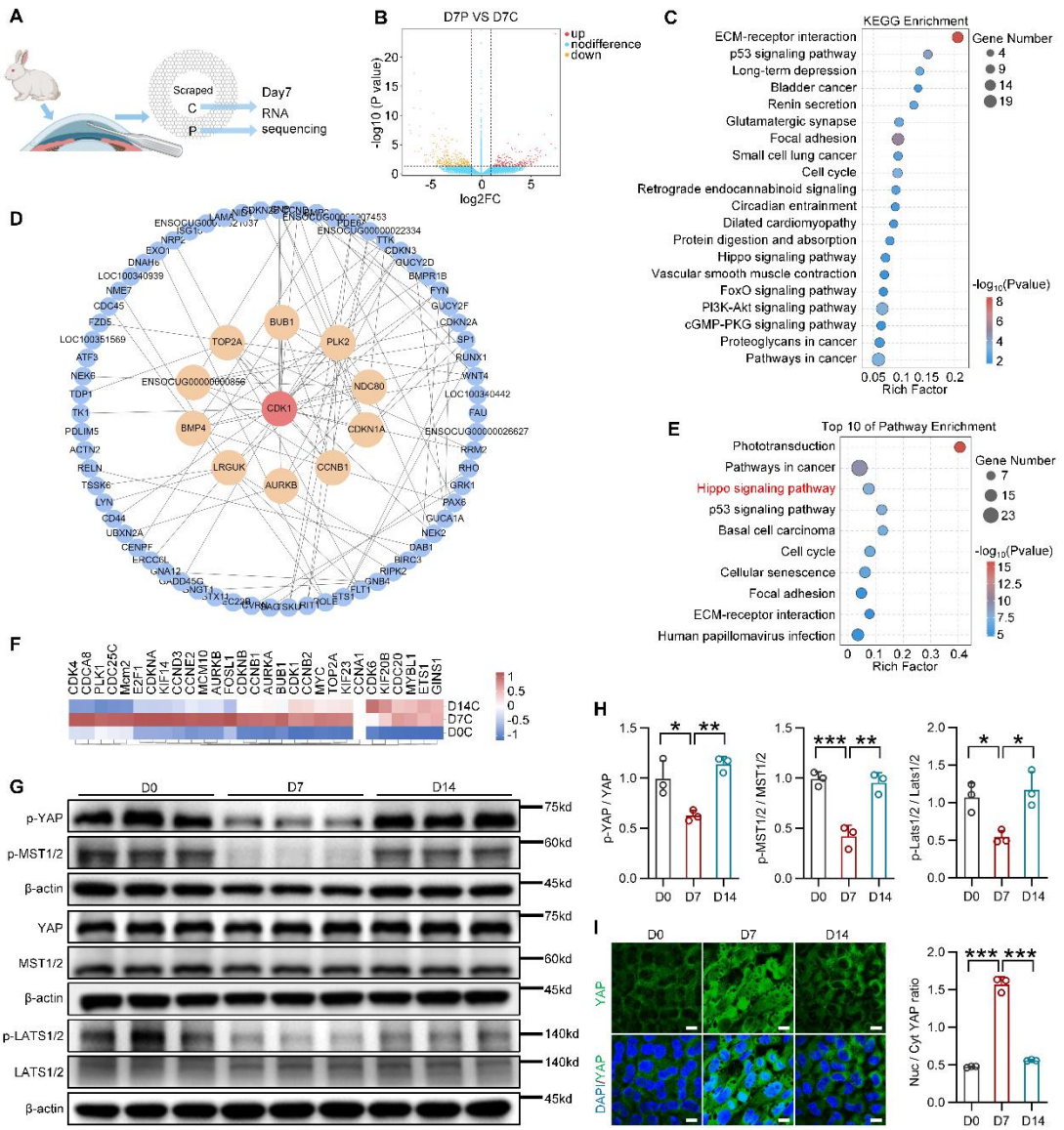

Fig.1. Transcriptomic analysis implicates Hippo pathway in CEC regeneration. (A) Diagram showing the experimental design. Rabbits central and peripheral CECs were taken for RNA sequencing separately on day 7 after injury. (B) Volcano plot of the significant DEGs between the central and peripheral CECs. (C) The KEGG enrichment of DEGs in (B). (D) The core proteins of the top 100 PPIs. (E) The top 10 of KEGG enrichment for genes related to the top 100 of PPIs in (D). (F) The heatmap of downstream genes of the Hippo pathway. (G, H) Western blot analysis of p-YAP, YAP, p-MST1/2, MST1/2, p-LATS1/2, LATS1/2 and β-actin, the protein levels were quantified by densitometry (n=3). (I) Representative immunofluorescence images of YAP and the ratio of nuclear YAP to cytoplasm YAP, five cells were randomly selected for measurement and averaged in each sample (n = 3). *P < 0.05, **P < 0.01, ***P < 0.001, error bars, mean ± SEM. Scale bars represent 10 μm in (I). Nuc, nucleus; Cyt, cytoplasm.

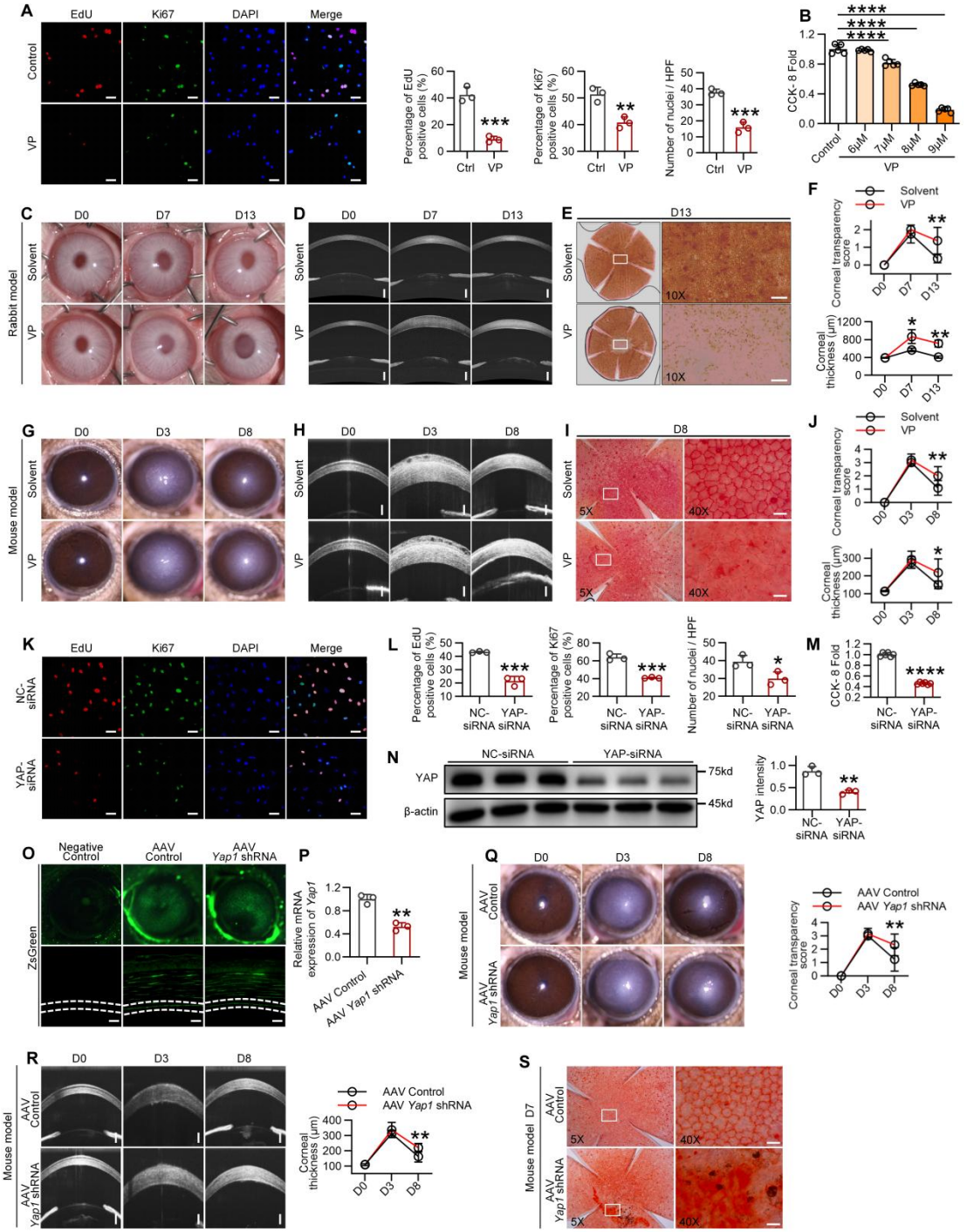

654

655 **Fig.2. Pharmacological YAP inhibition and knockdown of Yap1 suppressed CEC**
656 **regeneration.** (A) Representative staining images of primary rabbit CECs and percentage of
657 EdU and Ki67 positive cells and counting of DAPI (n = 3). (B) CCK-8 assay of primary
658 rabbit CECs. (C to E) Representative slit-lamp images (C), anterior segment OCT images (D)
659 and corneal alizarin red staining images (E) of rabbits. (F) Corneal transparency score and
660 central corneal thickness of rabbits (n = 4). (G to J) Representative images (G to I) and
661 corneal transparency score and central corneal thickness of mouse models (n = 5) (J). (K and
662 L) Representative images (K) of EdU and Ki67 and percentage of EdU, Ki67 positive cells

and counting of DAPI (n = 3) (L). (M) CCK-8 assay of primary rabbit CECs. (Fold of control, n = 6). (N) Western blot analysis of YAP in primary rabbit CECs (n = 3). (O) ZsGreen expression in vivo and in corneal sections. (P) Relative mRNA expression of Yap1 in mice corneal endothelium (n = 3). (Q) Representative slit-lamp images and corneal transparency score of mice (n = 6). (R) Representative anterior segment OCT images and central corneal thickness of mouse models (n = 6). (S) Representative corneal alizarin red staining images of mice. *P < 0.05, **P < 0.01, ***P < 0.001, ****P < 0.0001, error bars, mean ± SEM. Scale bars represent 500 μm in (D), 200 μm in (E), 100 μm in (H and R), 50 μm in (A and K), 25 μm in (O), and 20 μm in (I and S). VP, verteporfin.

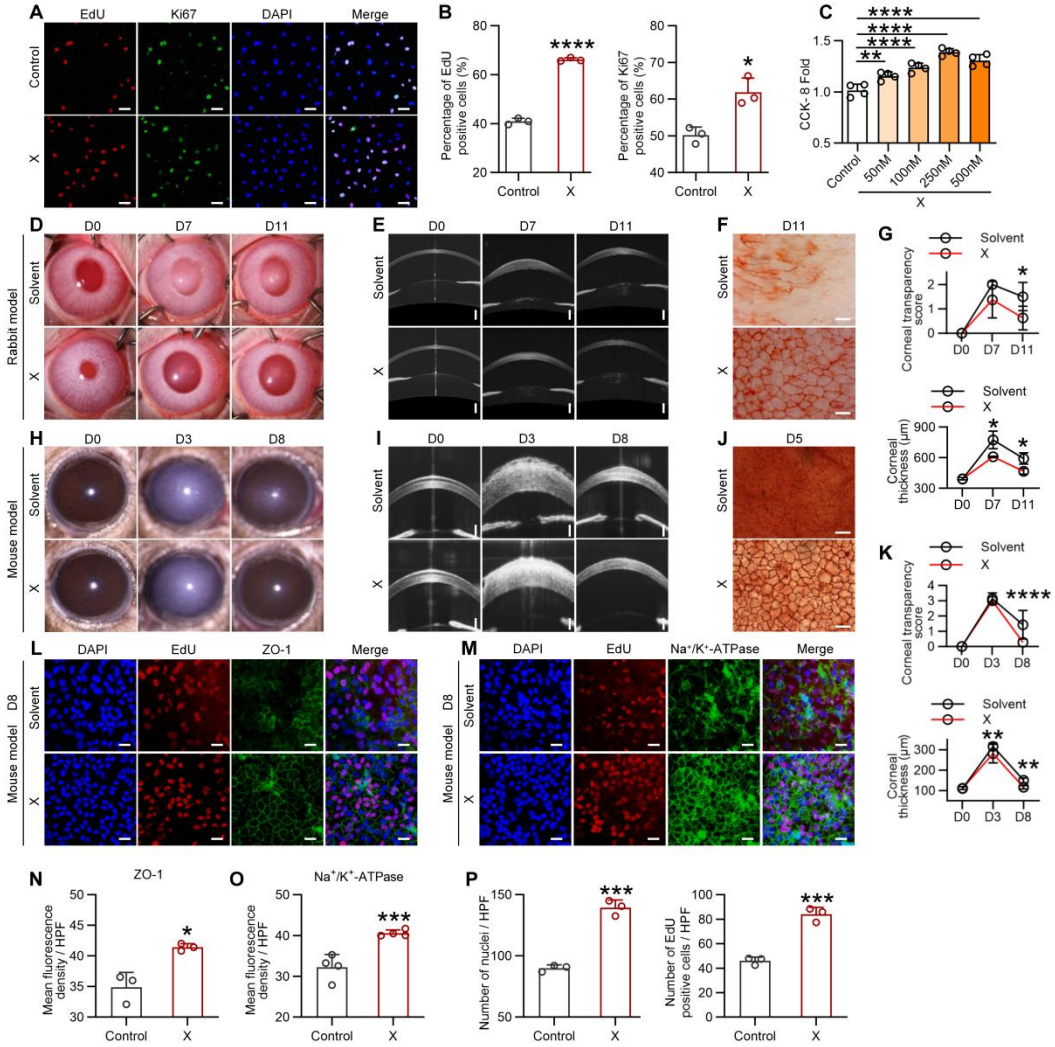

673

674 **Fig.3. XMU-MP-1 promotes CEC regeneration in rabbit and mouse models.** (A and B)
675 Representative staining images of primary rabbit CECs and percentage of EdU and Ki67
676 positive cells (n = 3). (C) CCK-8 assay of primary rabbit CECs (fold of control, n=4). (D to G)
677 Representative images (D to F) corneal transparency score and central corneal thickness of
678 rabbit models (n = 3) (G). (H to K) Representative images (H to J) and corneal transparency
679 score and central corneal thickness of mouse models (n = 6) (K). (L and M) EdU staining and
680 immunofluorescence of ZO-1 (L), Na^+-K^+ ATPase (M) of corneal endothelial whole mount.
681 (N and O) The intensities of ZO-1 (N) and Na^+-K^+ ATPase (O) (n = 3). (P) Quantification of
682 EdU positive cells and nuclei counting in (L and M) (n = 3). *P < 0.05, **P < 0.01, ***P <
683 0.001, ****P < 0.0001, error bars, mean ± SEM. Scale bars represent 500 μm in (G), 100 μm
684 in (I), 50 μm in (A), 25 μm in (L and M) and 20 μm in (F and J). X, XMU-MP-1; ip,
685 intraperitoneal injection.

686

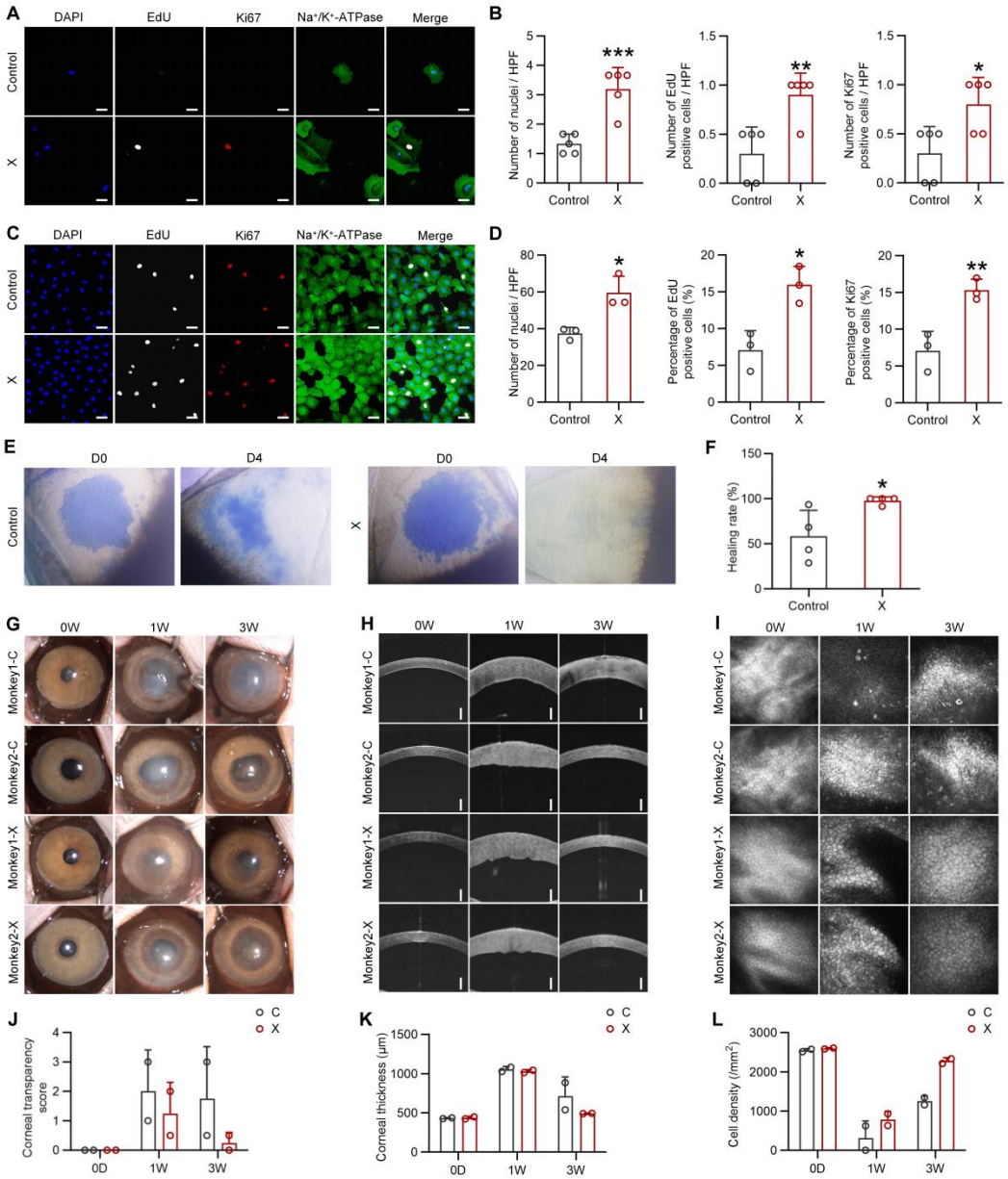

Fig.4. XMU-MP-1 promotes CEC regeneration in non-human primate. (A) EdU and DAPI staining and immunofluorescence of Ki67, Na^+-K^+ATPase in primary human CECs. (B) Nuclei counting and percentage of EdU and Ki67 positive cells in (A) (n = 5). (C) EdU and DAPI staining and immunofluorescence of Ki67 and Na^+-K^+ ATPase in primary monkey CECs. (D) Nuclei counting and percentage of EdU and Ki67 positive cells in (C) (n = 3). (E and F) Trypan blue staining of monkey corneal endothelium explants and the healing rate quantified by stained area (n=4). (G to I) Slit-lamp images (G), anterior segment OCT images (H) and corneal endothelial in vivo confocal microscope graphs (I) of monkeys. (J to L) Corneal transparency score (J), central corneal thickness (K) and central CECs density (L) of monkeys (n=2). *P < 0.05, **P < 0.01, ***P < 0.001, ****P < 0.0001, error bars, mean ± SEM. Scale bars represent 500 μm in (H) and 25 μm in (A and C). C, control; X, XMU-MP-1.